13

Seismic Protection of Monolithic Objects of Art Using a Constrained Oscillating Base

Alessandro Contento and Angelo Di Egidio
Department of Structural, Hydraulic and Geotechnical Engineering, University of L'Aquila
Italy

1. Introduction

The model of rigid block is well known in literature. In the past, several papers analyzed the behaviour of rigid blocks under different kind of excitations because many monolithic objects of art, such as statues, obelisks and fountains, subject to earthquake excitation, can be modelled as rigid blocks. In [Shenton & Jones, 1991] a general bi-dimensional formulation of the rigid block has been obtained and rocking and slide-rock approximated conditions have been written. More recently this model has been used to describe the behaviour of monolithic bodies subject to base excitations as a one-sine pulse excitation in [Zhang & Makris, 2001; Makris & Black, 2004, Kounadis 2010] and earthquake excitation in [Agbabian et al., 1988; Pompei et al, 1998; Taniguchi, 2002]. Almost all the papers on rigid blocks subject to base excitation focus their attention on symmetric rigid bodies. Only a few papers concern non-symmetric rigid bodies that, usually, represent objects of art better than symmetric rigid blocks. In [Boroscheck & Romo, 2004] the influence of the eccentricity of the centre of mass on the motion of the system has been studied. In [Purvance, 2005; Purvance et al., 2008] an analytical and experimental estimation of overturning events under seismic excitations has been carried out, both for symmetric and non-symmetric rigid bodies. In particular, in [Zhang & Makris, 2001] for a one-sine pulse excitation and in [Purvance, 2005; Purvance et al., 2008] for seismic excitation, the existence of survival regions that lie above the *PGA* (Peak Ground Acceleration) associated with the first overturning occurrence have been shown. In recent years, methods to reduce the effects of seismic excitation on art objects have been studied in some papers. In [Fujita et al, 2008] a critical excitation problem for a rigid block subjected to horizontal and vertical simultaneous base inputs is considered. In [Vestroni & Di Cinto, 2000] a base isolation system has been used to protect statues from seismic effects. The work of art has been modeled through an equivalent elastic beam. In [Caliò & Marletta, 2003] the same problem has been analyzed, but the art object has been modeled as a symmetric rigid block simply supported on an oscillating base connected to the ground by a visco-elastic device. The sliding of the body is prevented by special seismic restraints. These analyses have shown the effectiveness of the isolation system and the role of many parameters. To make things more realistic, in [Contento & Di Egidio, 2009], the model presented in [Caliò & Marletta, 2003] has been enriched considering also the eccentricity of the centre of mass of the rigid body and the presence of security stops, able to prevent the breaking of the isolation device by limiting

the displacement of the oscillating base to a maximum safety value. More recently, in [Di Egidio & Contento, 2009; Di Egidio & Contento, 2010], they have introduced sliding effects, that make the model able to carry out more complicated motions like slide-rocking, and sliding constrains, that prevent the rigid body from falling off the base. Alternatively, the possibility for the rigid block to be partially removed from the oscillating base has been considered. Security stops to avoid damaging the base isolation system are also considered. The behaviour of the whole system is studied under two types of excitations: impulsive and seismic. Exact nonlinear equations of motion are written for the different phases of motion: full-contact, sliding, rocking, slide-rocking; transition phase conditions are obtained by generalizing to the case under analysis those obtained in [Taniguchi, 2002; Caliò & Marletta, 2003; Contento & Di Egidio, 2009]. To describe the motion when the body is outside the oscillating support, original equations of motion, describing the rocking and the slide-rocking motions of the rigid block around a different point from one of the corners of its base, are obtained. The influence of the friction coefficient, of the eccentricity, of the security stops and of other parameters are analyzed by performing an extensive parametric analysis via a direct numerical integration of the equations of motion. Comparison between results obtained for isolated rigid body and non-isolated rigid body are also carried out to show the effectiveness of base isolation with respect to the absence of this passive control system. Another possibility, not considered here, is the use of three-dimensional models of rigid blocks, mostly circular based. They are used to study the sloshing in circular shaped tanks [Taniguchi, 2004], the wobbling motion [Stefanou et al., 2011] and the motion of a disk of finite thickness on a planar surface [Koh & Mustafa, 1990; Batista 2006].

2. Description of the object considered and model hypotheses

The two-dimensional model presented is that of an isolated rigid body, where the isolation system is an oscillating base connected to the ground by a linear visco-elastic device. The geometric dimensions of the rigid body are taken with ratios similar to those of real works of art and its characteristics are reported in Fig.1(a). With respect to the traditional models presented in literature, here, also the eccentricity of the centre of mass of the rigid body is considered: being C and O the centres of mass of the body and of the base respectively and M the middle point of the base, the eccentricity $e = b_1 - b$ is positive when the vertical projection of the centre of mass C is shifted on the right side of M. In Fig.1(b) parameters characterising the base isolation are shown, where c and k are the damping and the stiffness of the linear visco-elastic device representing the base isolation system.

The rigid body here considered can undergo different kinds of motion: (a) full-contact motion where the rigid body remains in contact with the isolated base when it oscillates, (b) sliding motion where the rigid body slides on the oscillating base, (c) rocking motion where the rigid body rocks around one of the two bottom corners without sliding and (d) slide-rocking motion where a combination of rocking and sliding motion occurs (Fig.2). Three Lagrangian parameters are used to describe the different phases of motion (Fig.2): $u(t)$ that is the translation of the oscillating base, $x(t)$ that is the translation of the body due to slide with respect to the isolated base and $\vartheta(t)$ that is the rotation of the body around one of the bottom corners and can be positive or negative if the body rocks around the left or the right corner respectively. Quantities u_g and v_g, shown in Fig.1(b), are the horizontal and vertical ground displacements respectively. Since there are no constraints the rigid block can come partially away from the base so that the rocking motion can occur not only around one of

the corners of the rigid body but also around one of the corners of the isolating base. For the same reason one of the possible collapse condition of motion is the body falling off the base. The other is the overturning of the body. In the model, frictional forces are expressed by using the Coulomb description and the friction coefficient has been varied in the different analyses carried out.

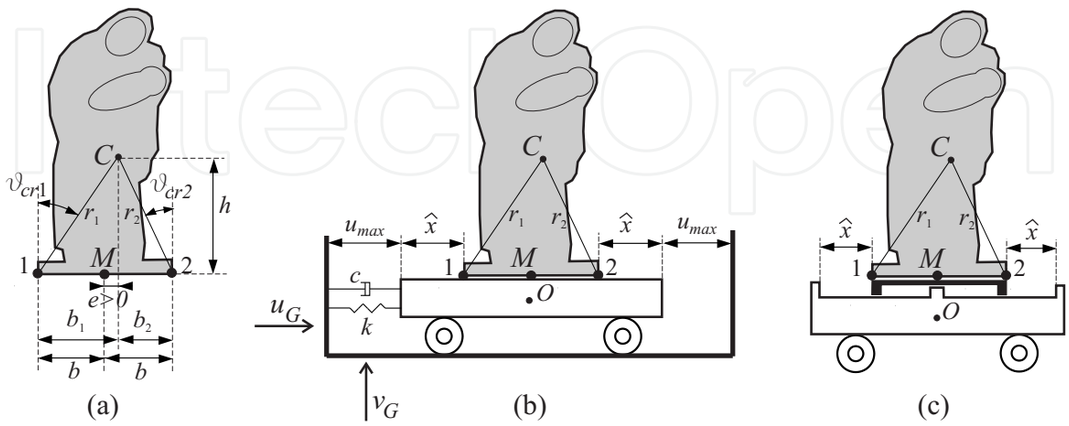

Fig. 1. Mechanical system: (a) geometrical parameters of the rigid body; (b) parameters of the base isolation system without security stops for the sliding motion; (c) security stops for the sliding motion.

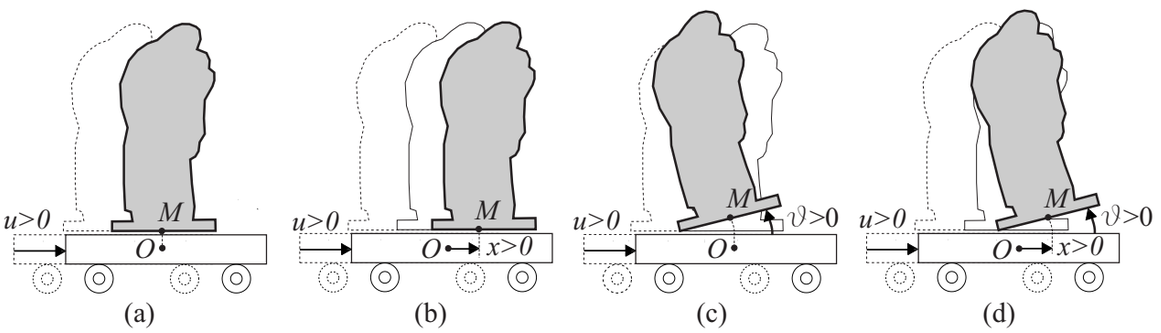

Fig. 2. Phases of motion: (a) full-contact; (b) sliding; (c) rocking; (d) slide-rocking.

3. General formulation

In this section the equations of motion for the different phases of motion, the transition conditions among them and the impact conditions are derived.

3.1 Equations of motion

Exact nonlinear equations of motion are written by using a Lagrangian approach for the different phases of motion.

3.1.1 Full-contact motion

The full-contact motion equation is the linear equation of a single degree of freedom system that represents the equilibrium of all forces acting on the system in the horizontal direction:

$$(m+m_b)(\ddot{u}+\ddot{u}_G)+c\dot{u}+ku=0 \tag{1}$$

where m and m_b are the mass of the rigid block and the mass of the isolated base, respectively.

3.1.2 Sliding motion

During a pure sliding motion kinetic energy T and potential energy V of the system can be written respectively:

$$T=\frac{1}{2}m\dot{u}_C^2+\frac{1}{2}m_B\dot{u}_O^2; \qquad V=\frac{1}{2}k(u_O-u_G)^2 \tag{2}$$

where u_c and u_o are the positions of the centres of the body C and of the base O expressed as functions of two Lagrangian parameters (Fig.3(a)):

$$u_C(t)=u_G(t)+u(t)+x(t), \qquad u_O(t)=u_G(t)+u(t) \tag{3}$$

Lagrange's equations of motion are derived as follows:

$$\begin{gathered} m(\ddot{u}+\ddot{u}_g+\ddot{x})+F=0 \\ (m+m_b)(\ddot{u}+\ddot{u}_g)+m\ddot{x}+c\dot{u}+ku=0 \end{gathered} \tag{4}$$

where F is the Coulomb kinetic friction force given by:

$$F=\mu_k\, sign(\dot{x})\, m(g+\ddot{v}_g) \tag{5}$$

and where μ_k is the kinetic friction coefficient and g the gravity acceleration.

3.1.3 Rocking motion

For the rocking motion, due to the fact that the model is non-symmetric, two different sets of equations of motion are necessary, depending on which corner the motion occurs. When the relative displacement $x\in[-\hat{x},\hat{x}]$, the base of the body is inside the oscillating support (see Fig.1(b)). In this case the positions of the centres of the rigid body C and of the base O, when a rocking around the corner 1 occurs, can be obtained by referring to Fig.3(b):

$$\begin{gathered} u_C(t)=u_G(t)+u(t)+(b_1'-\hat{b}_1) \\ v_C(t)=v_G(t)+(h_1'-h) \\ u_O(t)=u_G(t)+u(t) \end{gathered} \tag{6}$$

Kinetic energy, potential energy and vitual work δW of the non-conservative forces then read:

$$\begin{gathered} T=\frac{1}{2}m(\dot{u}_C^2+\dot{v}_C^2)+\frac{1}{2}m_b\,\dot{u}_O^2+\frac{1}{2}I_C\dot{\vartheta}^2; \\ V=\frac{1}{2}k\,u^2+m\,g\,(h_1'-h); \\ \delta W=-c\,\dot{u}(t)\,\delta u. \end{gathered} \tag{7}$$

Lagrange's equations of motion read:

$$\begin{aligned}(m+m_b)(\ddot{u}+\ddot{u}_G)+c\dot{u}+ku-m\ddot{\vartheta}h_1'-m\dot{\vartheta}^2b_1'=0\\ I_1\ddot{\vartheta}-m(\ddot{u}+\ddot{u}_G)h_1'+m(g+\ddot{v}_G)b_1'=0\end{aligned} \tag{8}$$

where

$$b_1'=\hat{b}_1\cos(\vartheta)-h\sin(\vartheta);\ h_1'=\hat{b}_1\sin(\vartheta)+h\cos(\vartheta) \tag{9}$$

are the horizontal and vertical distances between centre of mass and corner 1 (that is the centre of rotation) in the actual position, after rotation (see Fig.3(b)), and where $\hat{b}_1=b_1$ (see Fig.1(a)). In Eqs.(8) $I_1:=I_C+mr_1^2$ is the polar inertia around corner 1; I_C is the polar inertia with respect to centre *C* of the body. The first equation of motion of Eqs.(8) represents the equilibrium of the forces acting on the body together with the base in the horizontal direction, while the second represents the equilibrium of the moments around the corner on which the rotation occurs.

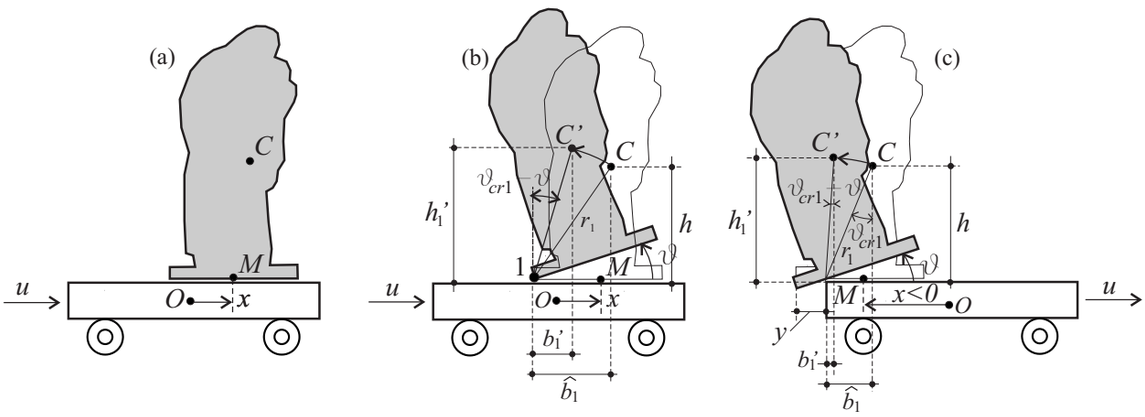

Fig. 3. Geometrical description of the different phases of motion: (a) sliding; (b) (slide-) rocking around corner 1; (c) (slide-)rocking where the left corner of the body is outside the oscillating base.

When the variable $x\notin[-\hat{x},\hat{x}]$, the base of the rigid body is outside the oscillating support. In this case the centre of rotation of the body is located in one of the corners of the oscillating support (see Figs. 3(c)). The positions of the centres of the rigid body *C* and the base *O*, when a rocking around the left corner of the support occurs ($-\hat{x}>x$), are equal to Eqs.(6) where, however, $\hat{b}_1=b_1+y$ with $y=x+\hat{x}$ ($x<0$ not depending on time, see Fig.3(c)). By using Eqs.(7) it is possible to obtain Lagrange's equations of motion equal to Eqs.(8). In this case I_1 is the polar inertia around the left corner of the support; b_1' and h_1' represent the horizontal and vertical distances between the centre of mass and the left corner of the oscillating support (and not the left corner of the rigid body as in the previous case, see Fig.3(c)). They are still given by Eqs.(9). The equations of motion of rocking around the right corner of the base or of the support can be obtained in a similar way (cases $x\in[-\hat{x},\hat{x}]$ and $x>\hat{x}$ respectively).

3.1.4 Slide-rocking motion

Also for the slide-rocking motion, due to the non-symmetry of the rigid body, two different sets of equations of motion are necessary, depending on which corner the rotation occurs. When during the motion the relative displacement $x \in [-\hat{x}, \hat{x}]$, by evaluating kinetic and potential energies and taking into account the virtual work of the generalized forces given by Eq.(7), Lagrange's equations of motion around the left corner can be found and read:

$$\begin{gathered} m(\ddot{u} + \ddot{u}_G + \ddot{x}) - m\ddot{\vartheta}h_1' - m\dot{\vartheta}^2 b_1' + F_1 = 0 \\ (m + m_b)(\ddot{u} + \ddot{u}_G) + m\ddot{x} + c\dot{u} + ku - m\ddot{\vartheta}h_1' - m\dot{\vartheta}^2 b_1' = 0 \\ I_1\ddot{\vartheta} - m(\ddot{u} + \ddot{u}_G + \ddot{x})h_1' + m(g + \ddot{v}_G)b_1' = 0 \end{gathered} \tag{10}$$

where b_1' and h_1', given by Eqs.(9), are the horizontal and vertical distances between the centre of mass and corner 1 (that is the centre of rotation) in the actual position, after rotation (see Fig.3(b)), and where $\hat{b}_1 = b_1$. Eq.(10_1) represents the equilibrium in the horizontal directions of all the forces acting on the rigid body (Fig.4(b)), while Eqs.(10_2) and (10_3) have the same meaning of Eqs.(8). The Coulomb kinetic friction force F_1 is given by:

$$F_1 = \mu_k \, sign(\dot{x}) Y_1 \tag{11}$$

where the vertical reaction Y_1 can be obtained by evaluating the vertical component of the total force acting on the rigid body (Fig.4(b)):

$$Y_1 = m(g + \ddot{v}_G) + mb_1'\ddot{\vartheta} - mh_1'\dot{\vartheta}^2 \tag{12}$$

The equations of motion of rocking around corner 2, in the case in which the relative displacement $x \in [-\hat{x}, \hat{x}]$ can be obtained similarly.

When the variable $x \notin [-\hat{x}, \hat{x}]$, the centre of rotation of the body is located in one of the corners of the oscillating support (see Fig.3(c)). It is possible to obtain Lagrange's equations of motion for the left corner:

$$\begin{gathered} m(\ddot{u} + \ddot{u}_G)\cos(\vartheta) + m\ddot{x} + m(g + \ddot{v}_G)\sin(\vartheta) - m\ddot{\vartheta}h - m\dot{\vartheta}^2\hat{b}_1 + F_1 = 0 \\ (m + m_b)(\ddot{u} + \ddot{u}_G) + m\ddot{x}\cos(\vartheta) + c\dot{u} + ku - m\ddot{\vartheta}h_1' - m\dot{\vartheta}^2 b_1' - 2m\dot{x}\dot{\vartheta}\sin(\vartheta) = 0 \\ I_1\ddot{\vartheta} - m(\ddot{u} + \ddot{u}_G)h_1' - m\ddot{x}h + m(g + \ddot{v}_G)b_1' + 2m\dot{x}\dot{\vartheta}\hat{b}_1 = 0 \end{gathered} \tag{13}$$

In this case I_1 is the polar inertia around the left corner of the support; b_1' and h_1' represent the horizontal and vertical distances between the centre of mass *C* and the left corner of the oscillating support (and not the left corner of the rigid body as in the previous case, see Fig.3 (c)). They are still given by Eqs.(9). It is interesting to observe that the first of Eqs.(13) represents the equilibrium of the forces acting during the slide-rocking motion along the slide direction parallel to the base of the body, when it is in a rotated configuration. The interpretation of the other two equations of motion do not change with respect to the previous case. A representation of the forces acting on the system during the slide-rocking motion around the left corner of the support is reported in Fig.4(c). The kinetic friction force

F_1 is still given by Eq.(11) where Y_1 represents the total force orthogonal to the inclined slide direction and it can be obtained by the forces acting on the rigid body (Fig.4(c)):

$$Y_1 = m(g+\ddot{v}_G)\cos(\vartheta) - m(\ddot{u}+\ddot{u}_G)\sin(\vartheta) + 2m\dot{x}\dot{\vartheta} + m\hat{b}_1\ddot{\vartheta} - mh\dot{\vartheta}^2 \tag{14}$$

It is interesting to observe that in this case the Coriolis force $(-2m\dot{x}\dot{\vartheta})$ appears in the system due to the fact that the centre of rotation of the rigid body changes its position with respect the body during the motion.

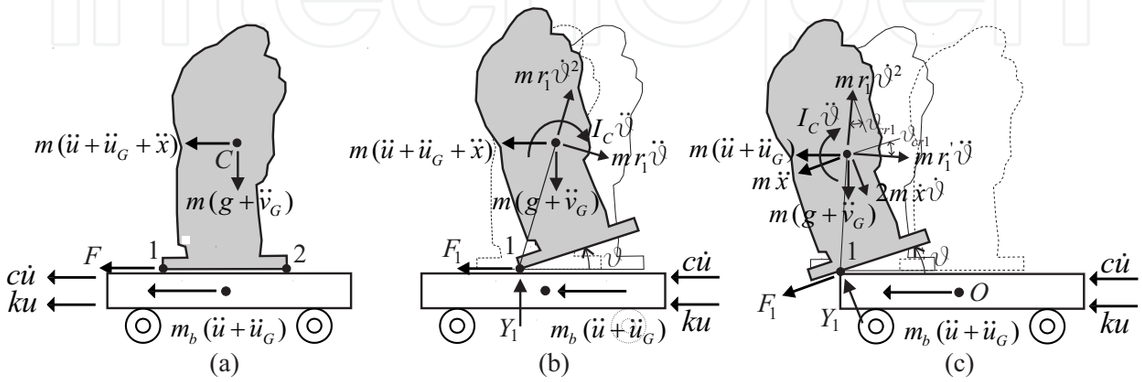

Fig. 4. Forces acting on rigid body: (a) during a sliding motion; (b) during (slide-)rocking around corner 1; (c) during (slide-)rocking where the left corner of the body is outside the oscillating base.

3.2 Transition and termination conditions

Transition phase conditions are obtained by the equilibrium among forces or moments acting on the rigid body during the motion. In the following only the case related to motions around the left corner is presented while transition and termination conditions evaluated for a motion occurring around the right corner can be found similarly.

3.2.1 Sliding motion

A pure sliding phase can take place starting from the rest or from the full-contact phase. By referring to the forces acting on the system during a full-contact phase shown in Fig.4(a) with $\ddot{x}=0$, a sliding phase can occur when the static frictional force $F_s = \mu_s m(g+\ddot{v}_G)$ is lesser than, or equal to, the absolute value of the horizontal inertial force $m(\ddot{u}+\ddot{u}_G)$. This condition reads:

$$\mu_s(g+\ddot{v}_G) \le \left|\ddot{u}+\ddot{u}_G\right| \tag{15}$$

where μ_s is the static friction coefficient. Equation (15) refers to starting condition from the rest when $\ddot{u}=0$ at $t=0$.

It is assumed that the termination condition of a sliding phase corresponds to the vanishing of the sliding velocity $|\dot{x}|=0$.

3.2.2 Rocking motion

The pure rocking phase can take place from the rest or the full-contact phase. A rocking phase can occur when the resisting moment M_R due to the vertical accelerations $m(g+\ddot{v}_G)$ of the body is smaller than the overturning moment M_O due to inertial force $m(\ddot{u}+\ddot{u}_G)$ (see Fig.4(a) with $\ddot{x}=0$). Considering the moments around the left corner (of the body or of the support), the following equation can be obtained:

$$\ddot{u}+\ddot{u}_G \geq \frac{\hat{b}_1}{h}(g+\ddot{v}_G) \tag{16}$$

where $\hat{b}_1 = b_1$ when the relative displacement $x \in [-\hat{x}, \hat{x}]$ during the full-contact motion, (see Fig.3(b)). On the contrary if the relative displacement $-\hat{x} > x$, then $\hat{b}_1 = b_1 + y$ with $y = x + \hat{x}$ ($x < 0$, see Fig.3(c)). Equation (16) refers to a starting condition from the rest when $\ddot{u}=0$ at $t=0$ (and $x=0$). There is a favoured direction for the beginning of the rocking phase associated with the sign of the total acceleration $\ddot{u}+\ddot{u}_G$. In some cases when $\hat{b}_1 = 0$ or $\hat{b}_2 = 0$, which are the cases where the centre of mass is placed on the vertical projection of the centre of rotation of the body, an unstable equilibrium position manifests itself.

No particular conditions are assumed to describe the termination condition of a rocking phase. This means that the rocking phase finishes when the energy associated to this phase is completely dissipated.

3.2.3 Slide-rocking motion

A slide-rocking motion can take place following the rest condition, the full-contact phase, the pure sliding phase or the pure rocking phase. Depending on which phase it starts, different starting conditions must be considered. First the starting condition of a rocking phase during a sliding motion will be analyzed. By referring to forces acting on the system during a sliding phase shown in Fig.4(a), a rocking phase can occur when the resisting moment M_R due to the vertical accelerations $m(g+\ddot{v}_G)$ of the body is smaller than the overturning moment M_O due to inertial force $m(\ddot{u}+\ddot{u}_G+\ddot{x})$. Considering the moments with respect to the left corner (of the body or of the support), the following equation can be obtained:

$$\ddot{u}+\ddot{u}_G+\ddot{x} \geq \frac{\hat{b}_1}{h}(g+\ddot{v}_G) \tag{17}$$

where, if the displacement $x \in [-\hat{x}, \hat{x}]$, then $\hat{b}_1 = b_1$ (se Fig.3(b)); if the relative displacement $-\hat{x} > x$, then $\hat{b}_1 = b_1 + y$ with $y = x + \hat{x}$ ($x < 0$, see Fig.3(c)). There is a favoured direction for the beginning of the rocking phase also in this case. The starting condition of a sliding phase during a rocking motion can be evaluated by referring to the forces acting on the rigid body during a rocking motion shown in Fig.4(b) with $\ddot{x}=0$. When the body is rocking around the left corner (of the body or of the support), the starting condition for a slide can be easily written as:

$$\mu_s Y_1 \leq |X_1| \tag{18}$$

where X_1 and Y_1 are the reactions of the base as in Fig.4(b),(c). If the displacement $x \in [-\hat{x}, \hat{x}]$, force Y_1 is given by Eq.(12), while X_1 can be evaluated by computing the total horizontal force acting on the rigid body. By referring to forces in Fig.4(b) (with $\ddot{x} = 0$), it reads:

$$X_1 = m(\ddot{u} + \ddot{u}_G) - mh_1'\ddot{\vartheta} - mb_1'\dot{\vartheta}^2 \tag{19}$$

When $-\hat{x} > x$, the force Y_1 is given by Eq.(14) with $\dot{x} = 0$, while X_1 can be evaluated by computing the total force acting on the rigid body along the sliding direction. By referring to forces in Fig.4(c) (with $\dot{x} = \ddot{x} = 0$), it reads:

$$X_1 = m(\ddot{u} + \ddot{u}_G)\cos(\vartheta) + m(g + \ddot{v}_G)\sin(\vartheta) - mh\ddot{\vartheta} - m\hat{b}_1\dot{\vartheta}^2 \tag{20}$$

Finally the starting condition of a slide-rocking phase from the full-contact phase is analyzed. A slide-rocking motion can take place from this phase if pure sliding and rocking conditions occur simultaneously. In particular a slide-rocking around the left corner (of the body or of the support) occurs when Eq.(15) and Eq.(16) are simultaneously proven. A slide-rocking phase takes place directly from the rest if the same previous equations, with $\ddot{u} = 0$ at $t = 0$, are simultaneously proven ($\hat{b}_1 = b_1$).

Also in this case, the termination condition of the sliding motion is taken to be $|\dot{x}| = 0$. When this condition is satisfied only the rocking motion remains active. The termination of the rocking motion is associated with the total dissipation of the energy associated to this phase; in this case only the sliding motion remains.

3.3 Impact conditions

Both during pure rocking motion and during slide-rocking motion an impact among the rigid block and the isolated base occurs when the angle ϑ approaches zero. No bouncing phenomenon is taken into account. Post impact quantities can be found, assuming that the impact happens instantly and the body position remains unchanged, imposing the conservation of the angular momentum and the conservation of the linear momentum along the horizontal direction. Referring to an impact that occurs when the object approaches the base by rocking around the left corner (of the body or of the support), the angular momentum after the impact $I_2\dot{\vartheta}^+ + mhu^+$ has to be equal to the angular momentum before the impact $I_1\dot{\vartheta}^- - 2mr_1b_2sin(\alpha_2)\dot{\vartheta}^- + mhu^-$. This condition reads:

$$I_1\dot{\vartheta}^- - 2mr_1bsin(\alpha_1)\dot{\vartheta}^- + mh\dot{u}^- = I_2\dot{\vartheta}^+ + mh\dot{u}^+ \tag{21}$$

where $r_1^2 = \hat{b}_1^2 + h^2$. The conservation of the linear momentum is needed to relate u^+ and u^- under the assumption that the impact (that happens instantly by hypothesis) does not affect the sliding motion:

$$mh\dot{\vartheta}^- + m(\dot{u}^- + \dot{x}) + m_b\dot{u}^- = mh\dot{\vartheta}^+ + m(\dot{u}^+ + \dot{x}) + m_b\dot{u}^+ \tag{22}$$

If the relative displacement $x \in [-\hat{x}, \hat{x}]$, then $\hat{b}_1 = b_1$ (see Fig.3(b)); if the relative displacement $-\hat{x} > x$, then $\hat{b}_1 = b_1 + y$ with $y = x + \hat{x}$ ($x < 0$, see Fig.3(c)). Taking Eq.(21) and

Eq.(22) into account, which means considering an impact that happens when the body is approaching the base by rocking around the left corner and successively rocking around the right corner, for a rectangular body, the following post-impact velocities are obtained:

$$\dot{\vartheta}^{+} = \frac{m^2h^2 - I_1(m+m_b) + 2mbr_1\sin(\alpha_1)(m+m_b)}{m^2h^2 - I_2(m+m_b)}\dot{\vartheta}^{-} \tag{23}$$

and

$$\dot{u}^{+} = \dot{u}^{-} + \frac{hm(I_1 - I_2 - 2bmr_1\sin(\alpha_1)}{h^2m^2 - I_2(m+m_b)}\dot{\vartheta}^{-} \tag{24}$$

The maximum value of the coefficient of restitution that allows rocking motion of a block on an isolated base then reads:

$$r_1 = \left(\frac{\dot{\vartheta}^{+}}{\dot{\vartheta}^{-}}\right)^2 = \left(\frac{m^2h^2 - I_1(m+m_b) + 2mbr_1\sin(\alpha_1)(m+m_b)}{m^2h^2 - I_2(m+m_b)}\right)^2 \tag{25}$$

In Fig.5 some values of the restitution coefficient are shown. The dashed and dotted lines represent r_1 obtained for $e = 0.3b$ and $e = -0.3b$ respectively, while the solid line represents $r_1 = r$ $(e = 0)$ as in [Vassiliou & Makris, 2011]. In the analyses the restitution coefficient has been taken accordingly with Eq.(25).

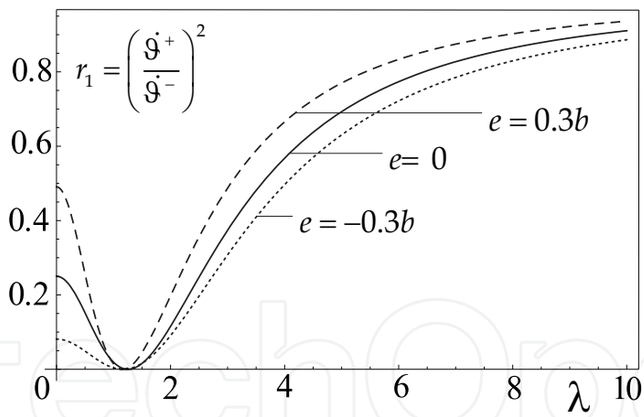

Fig. 5. Restitution coefficient for different values of the eccentricity.

4. Description of the excitations

Two types of base excitations are considered in the following: impulsive excitation and seismic excitation. Results are obtained in an analytical or in a numerical way depending on the excitation considered. Several geometrical and mechanical parameters are introduced to characterise the behaviour of the system. In particular:

$$\omega = \sqrt{\frac{k}{m+m_b}} \;\; ; \;\; T = \frac{2\pi}{\omega} \; ; \; \xi = \frac{c}{2(m+m_b)\omega} \tag{26}$$

where ω is the frequency, T is the period and ξ is the damping ratio of the isolated system in the full contact phase, that are well known quantities. Other quantities are introduced to characterize the system:

$$\varepsilon = \frac{e}{b} \;;\; \lambda = \frac{h}{b} ; \; \alpha = \frac{m_b}{m} \tag{27}$$

where ε is the eccentricity ratio with respect to the base of the rigid body, λ is the slenderness of the body and α is the mass ratio.

4.1 Impulsive excitation

An horizontal impulsive ground excitation has been considered. The solution of the full-contact, Eq.(1), under an impulsive ground acceleration I, can be found in closed form and is well known, so, in this case, most of the results have been found analytically. Since the system exhibits a symmetry in the rocking motion, conditions where there is a rocking motion have been evaluated only referring to a rocking around corner 1 and for and eccentricity $\varepsilon < 0$. Results are exposed trough maps describing the criteria for the different phases of motion. These maps, firstly obtained for non isolated, symmetric rigid body subjects to a horizontal ground acceleration in [Shenton, 1996], were successively extended to vertical ground acceleration in [Tung, 2007]. Here they are extended to base isolated non-symmetric rigid body subjects to a horizontal ground impulsive excitation and comparison between not isolated and isolated systems is carried out.

4.2 Seismic excitation

In this case the system has been excited with two different Italian registered seismic ground motions. Also for this kind of excitation only horizontal components of the seismic source

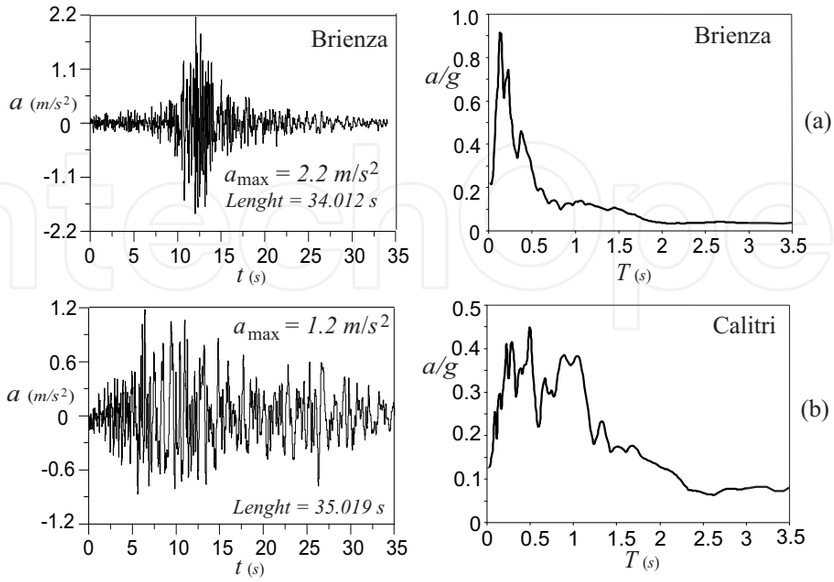

Fig. 6. Time-history and response spectrum of the Italian seismic accelerations used in the analysis: (a) Brienza; (b) Calitri.

$\ddot{u}_g(t) = \gamma f(t)$ are considered, where $f(t)$ is the recorded seismic acceleration and γ is a variable coefficient used to scale the maximum amplitude of the seismic accelerations (*PGA*: Peak Ground Acceleration). In Fig.6 the seismic inputs used and the time-histories with their elastic response spectrums are shown. The Brienza seismic source (Fig.6(a)) is used to analyze the behaviour of the isolated rigid block and its dependence on several parameters, especially on the friction coefficient; the Calitri seismic source (Fig.6(b)) is used to evaluate the influence of the spectral characteristic of the earthquake in the dynamics of the isolated system.

4.3 Description of the simulation

Results are obtained via a direct numerical integration of the equations of motion using a Runge-Kutta fourth order scheme. Special care is devoted to the choice of the integration time step and appropriate procedures are followed to iteratively identify the transitions among the different phases. Extensive parametric analyses are conducted to evaluate the influence of the friction coefficient, the eccentricity and the slenderness as well as the period of the isolated base on the behavior of the system. Analyses are performed by increasing the *PGA* or the impulsive excitation to find the first occurrence of rocking, sliding and falling or overturning of the body. Maps of behavior are produced to compare the results obtained with similar systems.

5. Description of the results

Results have been obtained for two different cases, the first one where only the rocking motion is allowed and a second one where the body is able to slip as well.

5.1 Introduction of safety devices

Two types of security stops have been introduced in the model considered and their effects on the system investigated. The first is able to prevent isolation device breakage by limiting the displacement of the oscillating base to a maximum safety value, the others are introduced to prevent the rigid body from falling off the base.

5.1.1 Security stops for the base isolation

This kind of security stops is introduced to prevent the breaking of isolation devices that generally cannot support displacements greater than a boundary value $u_{\max}$ (see Fig.1(b)). During the motion, if the velocity $\dot{u}$ is different from zero, an impact among oscillating base and security stops occurs when:

$$|u| = u_{\max} \tag{28}$$

To evaluate the condition after an impact, it is assumed that: the impact happens instantly and the body position remains unchanged; during the impact, a fraction of the horizontal momentum is dissipated and after the impact there is an inversion in the direction of motion. The horizontal momentum after the impact $Q_H^+ = (m + m_b)\dot{u}^+$ becomes a fraction η_i of the horizontal momentum before the impact $Q_H^- = (m + m_b)\dot{u}^-$. By letting $\left|Q_H^+\right| = \eta \left|Q_H^-\right|$, it is possible to obtain the post-impact velocity of the body:

$$\dot{u}^{+} = -\eta_i \dot{u}^{-} \tag{29}$$

where η_i is the restitution coefficient that can assume values in the range [0, 1].

5.1.2 Security stops for the slip of the body

Special sliding constrains that prevent the rigid body from falling off the base have been introduced in the model as an alternative to the possibility of the rigid block coming partially away from the base (Fig.1(c)). An impact among the body and the security stops, during a slide or a slide-rocking motion occurs when:

$$|x| = \hat{x} \tag{30}$$

if the velocity $\dot{x}$ is different from zero. After the impact it is supposed that the horizontal momentum due to slide motion $m\dot{x}^{-}$ completely vanishes since it is partially dissipated and partially transferred to the horizontal momentum of the oscillating base. In particular:

$$(m + m_b)\dot{u}^{-} + \eta_s m\dot{x}^{-} = (m + m_b)\dot{u}^{+} \tag{31}$$

from which it is possible to obtain the post-impact velocity of the base:

$$\dot{u}^{+} = \dot{u}^{-} + \eta_s \frac{m}{m + m_b}\dot{x}^{-} \tag{32}$$

where η_s is the restitution coefficient that can assume values in the range [0, 1], under the assumptions that the impact happens instantly.

5.2 Pure rocking motion

Analyses are performed to evaluate the first time at which rocking and overturning of the body occur. This evaluation is done for several values of parameters ε, T and λ. The analyses here performed do not permit to obtain the so-called survival regions that lies above the first overturning occurrence as in [Zhang & Makris, 2001; Purvance, 2005; Purvance et al., 2008].

5.2.1 Impulsive excitation

The rocking condition around corner 1 can be obtained by equating the maximum overturning moment $mh|\ddot{u}_{\max}|$, due to the inertia forces, with the resisting moment $mg(b+e)$, due to gravity, in which $|\ddot{u}_{\max}|$ is the absolute maximum acceleration generated by an impulse. This equation can be written, taking into account Eq.(27):

$$|\ddot{u}_{\max}| = \frac{g}{\lambda}(1+\varepsilon) \tag{33}$$

The solution of the full-contact equation (1), under an impulsive ground acceleration I, is well known and reads:

$$u(t) = \frac{I}{\omega}\frac{1}{\sqrt{1-\xi^2}} e^{-\xi\omega t} \sin(\omega t\sqrt{1-\xi^2}) \tag{34}$$

By solving a maximum problem, it is possible to obtain the absolute maximum acceleration:

$$\left|\ddot{u}_{\max}\right| = \left|I\right| \omega\, a(\xi) = \frac{2\pi \left|I\right|\, a(\xi)}{T} \tag{35}$$

where the function $a(\xi)$, which is always positive, reads:

$$\begin{aligned} a(\xi) &= 1 && \text{for } \xi = 0 \\ a(\xi) &= e^{-\frac{\xi}{\sqrt{1-\xi^2}}\operatorname{Arc\,tan}\left(\frac{\sqrt{1-\xi^2}}{\xi}\frac{1-4\xi^2}{3-4\xi^2}\right)} && \text{for } 0 < \xi \le \frac{1}{2} \end{aligned} \tag{36}$$

Starting rocking condition can be obtained by Eq.(16) (with $\ddot{u}_g = \ddot{v}_g = 0$), taking into account Eq.(35):

$$\mathcal{C}_R : \left|I\right| = \frac{T\, g}{2\pi\, a(\xi)}\frac{1}{\lambda}(1+\varepsilon) \tag{37}$$

In the following, with solid lines overturning curves are indicated, while with dashed lines rocking curves are indicated; moreover thin lines refer to an isolated rigid block, while thick lines refer to a non-isolated rigid block. In Fig.7(a) minimum rocking and overturning impulses versus the period of the isolated base *T* are plotted for a fixed damping ξ. In grey regions a rocking phase occurs. Below these regions only a full-contact phase is possible, while above an overturning of the rigid block occurs. It is observed that when *T* is increased the object rocks or overturns with higher impulse amplitude, however, the distance between the rocking and the overturning curves decreases. It is also possible to observe that for increased eccentricities the behaviour of the system worsens since smaller impulses are able to cause the rocking or the overturning. Also the amplitude of the rocking regions becomes smaller when the eccentricity is increased. In Fig.7(b) rocking and overturning impulses versus the eccentricity are shown both for isolated and non-isolated systems. Referring to the isolated system, also in this case, the grey area indicates the rocking phase region. The best behaviour of the system is obtained when $\varepsilon = 0$ (symmetric body); the presence of an eccentricity reduces the performances since a smaller impulse is required to cause rocking or overturning. When $\varepsilon = \pm 1$ (the centre of mass is located on a vertical side of the body), since no resisting moment is present, the system is in an unstable equilibrium position. By comparing rocking and overturning curves for isolated and non-isolated systems, it is possible to observe the efficiency of the base isolation. It has to be highlighted that the rocking curve for non-isolated system is coincident with the horizontal axis (the minimum rocking impulse is always zero) because, given that an impulse corresponds to an initial velocity, a non-isolated body has always to start its motion with an angular velocity $\dot{\vartheta}(0) \neq 0$. Finally in Fig.7(c) rocking and overturning impulses versus the slenderness λ are shown both for isolated and non-isolated systems. Curves are plotted starting by the value

of the slenderness $\lambda = 1/\sqrt{2}$ above which no bouncing phenomena occur. For a fixed eccentricity an increase of the slenderness causes an evident worsening of the behaviour. For higher values of the eccentricity both isolated and non-isolated systems reduce their performances. Grey region refers to rocking phase for $\varepsilon = \pm 0.5$, both for isolated and non isolated structure; an increasing of the eccentricity also causes a reduction in the dimensions of the rocking region.

5.2.2 Seismic excitation

In Fig.8 comparison between the behaviour of an isolated rigid body with and without security stops for the oscillating base is shown under Buia earthquake (security stops for the sliding are not considered here). In the vertical left side of the graphs the scale factor γ is reported, while in the vertical right side the *PGA* is reported.

In particular in Fig.8(a) rocking and overturning curves versus eccentricity ε are drawn in the case of absence of security stops (thick lines) and the case in which these safety devices are present (thin lines). Dotted thick line refers to impact events: it gives the scaling factor γ (or *PGA*) at which impacts on security stops occur for each value of eccentricity ε. It is possible to observe that after an impact rocking and overturning happens for a lower value of the scaling factor with respect to the case in which security stops are not considered. Time-histories of $u(t)$ and $\vartheta(t)$ show better what happens when an impact occurs (Fig.8(b),(c)). Also in these figures thick lines denote the absence of security stops while thin lines denote the presence of this safety device. For the case labelled with *H* in Fig.8(a), when the displacement of the oscillating base $u(t)$ reaches security stops ($|u(t)| = u_{\max}$) one or more successive impacts can occur, as shown in Fig.8(b). The angle of rocking $\vartheta(t)$ (Fig.8(c)) in general increases with respect to the case in which security stops are not considered and causes the overturning of the rigid body for lower values of the scaling factor. Quantity t_r refers to the time at which rocking phase starts, that is the instant at which Eq.(16) is satisfied.

In the following, when safety devices are introduced, these characteristics are always considered: $\eta = 0.70$, $u_{\max} = 0.20$. In Fig.9 comparison between isolated and non isolated system is shown to better evaluate the efficiency of the isolation system under Buia earthquake for a fixed damping and in presence of security stops. In particular in Fig.9(a) rocking and overturning curves versus the period *T* are plotted for several eccentricity ε. Dots on γ-axis refer to the behaviour of the non isolated system. It is possible to observe that increasing the level of the protection (that is increasing period *T*) scaling factors at which rocking occurs increase with respect to the non isolated system, instead overturning scaling factors do not monotonically grow with *T* due to the high nonlinearity of the system. For example the minimum of the overturning curve that occurs in the range $T \in (0.5, 1.0)$ is related to the high contents of spectral energy of the Buia earthquake in the same range. Out of this range, the isolated system requires higher scaling factors to cause the overturning of the rigid body with respect the non isolated system. The behaviour of the system significantly decays when the rigid body has an eccentricity different to zero. The grey area in the graph refers to the region in which a rocking phase occurs for $\varepsilon = 0.5$. Below this

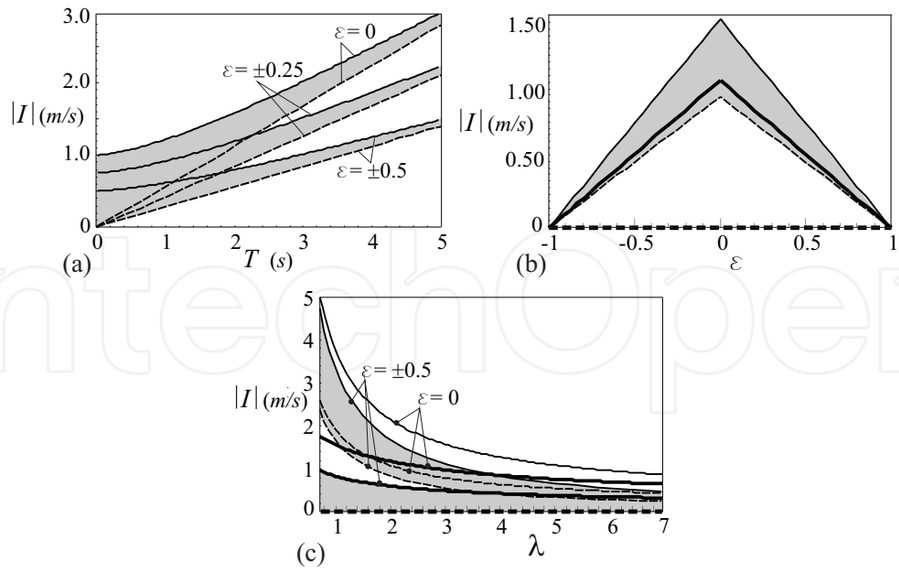

Fig. 7. Dependence on eccentricity ε : (a) Minimum absolute impulse versus period T ($\lambda = 3$); (b) Minimum absolute impulse versus eccentricity ε ($\lambda = 3,\ T = 2s$); (c) Minimum absolute impulse versus slenderness λ ($T = 2s$); ($b = 0.3m,\ \rho = 2000\,kg/m^3,\ \xi = 0.05$).

region a full-contact phase takes place; above this region an overturning of the rigid body occurs. In Fig.9(b) rocking and overturning curves versus the eccentricity ε are plotted. Thick lines refer to the non isolated system, while thin lines to isolated system. Rocking and overturning curves for isolated system are the same shown in Fig.8(a). It is possible to note that the best behaviour of the system is obtained when $\varepsilon = 0$ (symmetric body); the presence of an eccentricity reduces the performances since a smaller impulse is required to cause rocking or overturning. By comparing rocking and overturning curves for isolated and non-isolated systems, it is possible to observe the efficiency of the base isolation. Also in this case grey areas indicate the rocking phase regions. Below these areas there is no rocking, above them there is a critical region in which overturning is not guaranteed everywhere because of the existence of survival regions that lie above the curve associated with the first overturning occurrence. Finally in Fig.9(c) rocking and overturning curves versus the slenderness λ, for a fixed eccentricity ($\varepsilon = 0.5$), are plotted. Also in this figure thick lines refer to the non isolated system, while thin lines to isolated system. Also in this case curves are plotted starting by the value of the slenderness $\lambda = 1/\sqrt{2}$. By increasing the slenderness λ both the non isolated and the isolated systems generally show a decay of the performances, but it is possible to observe also in this case the greater efficiency of the base isolated system.

The thick dotted line is the impact curve. Also in this case grey areas indicate the rocking phase regions. It is useful to summarize the effects due to the presence of security stops. In Fig.8(a) it is possible to observe that a range of eccentricity ($|\varepsilon| < 0.75$), in which impact events have the greater effects, exists. Into this range, when an impact occurs before the rocking in the system without security stops, the impact and the rocking curves become practically coincident. This means that the impact is the principal cause of rocking. Instead, when an impact occurs after the rocking, the impact and the overturning curves become coincident. This means that the impact

is the main cause of overturning. This limit value of the absolute eccentricity seems to be possessed by every systems and it depends on geometrical and mechanical characteristics of the system itself. Also above a slenderness limit value ($\lambda > 3$) it happens that impact curve and overturning curve coincide, as shown in Fig.9(c). This slenderness limit value also depends on geometrical and mechanical characteristics of the system.

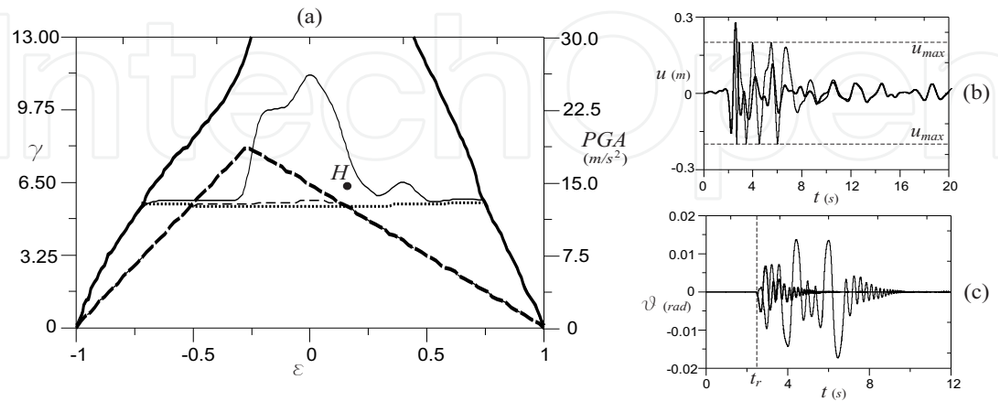

Fig. 8. Effects of the security stops under Buia earthquake: (a) Seismic scale factor versus eccentricity ε ($b = 0.3m$, $\lambda = 3$, $\rho = 2000 kg/m^3$, $\xi = 0.20$, $\eta = 0.70$, $u_{\max} = 0.20$, $T = 2s$); (b) Time history of displacements $u(t)$ for the case labelled with *H* in Fig.8a ($\varepsilon = 0.3$, $\gamma = 6.5$); (c) Time history of rotation $\vartheta(t)$ for the case labelled with *H*.

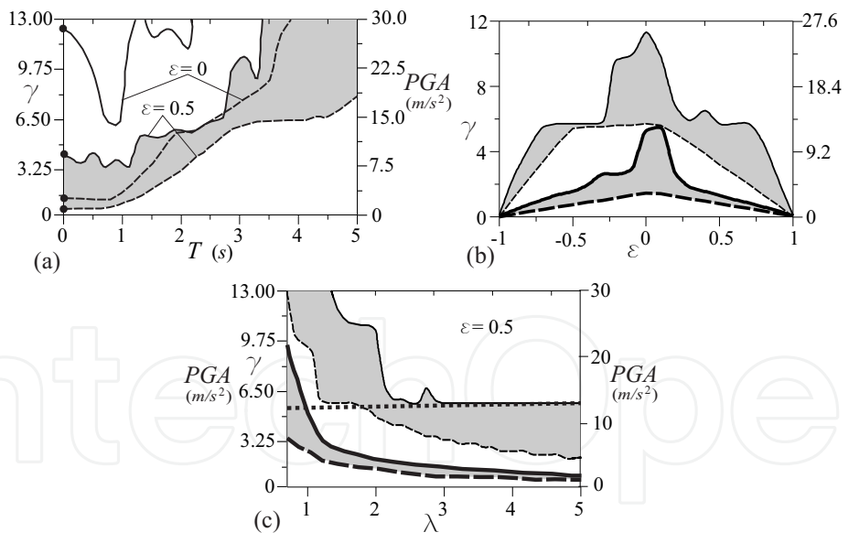

Fig. 9. Seismic analysis under Buia earthquake: (a) Seismic scale factor versus period *T* ($\lambda = 3$); (b) Seismic scale factor versus eccentricity ε ($\lambda = 3$, T = 2 s); (c) Seismic scale factor versus slenderness λ (T = 2 s); ($b = 0.3m$, $\rho = 2000 kg/m^3$, $\xi = 0.20$).

The last analysis reported here points out the effects of the spectral characteristics of the earthquake. A simplified analysis is conducted by using Brienza and Calitri Italian registered earthquakes (Fig.6(b),(c)) with comparable lengths both normalized by assuming an acceleration peak equal to *g*. In Fig.10(a) rocking and overturning curves, obtained by

evaluating for which slenderness λ the body rocks or overturns by varying the eccentricity ε, are plotted. It is clear that under Brienza earthquake the system shows a better behaviour since rocking and overturning happen for higher slenderness with respect to the Calitri earthquake. Grey areas indicate the rocking phase regions. Below these areas there is full-contact, above them there is overturning. In Fig.10(b) rocking (dashed lines) and overturning (solid lines) curves, obtained by evaluating the level of protection (that is the period T) to prevent rocking or overturning of the body by varying the eccentricity ε, are plotted. It is evident that the Brienza earthquake requires a lower level of protection with respect to the Calitri earthquake, to prevent rocking or overturning. For Brienza input in the range $\varepsilon \in [\varepsilon_A, \varepsilon_B]$, base isolation ($T = 0$) is not necessary to prevent overturning. Also in this case grey areas indicate the rocking phase regions but on the contrary, over these areas there is full-contact, below them there is a critical region in which overturning is not guaranteed everywhere because of the existence of survival regions. The isolated system shows a better behaviour for earthquake with a more narrow spectrum as found in [Purvance et al., 2008].

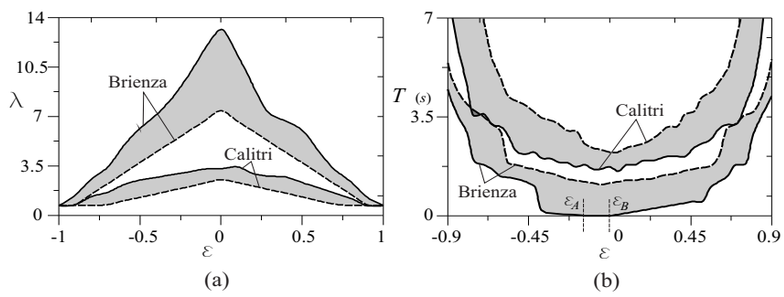

Fig. 10. Comparison between normalized Brienza and Calitri earthquakes (PGA=g): (a) slenderness λ versus eccentricity ε ($b = 0.3m$, $\lambda = 3$, $T = 2s$) and (b) period T versus eccentricity ε ($b = 0.3m$, $\lambda = 3$, $\rho = 2000 kg/m^3$, $\xi = 0.20$).

5.3 Slide-rocking motion

As for the rocking motion, analyses are performed to evaluate the first time at which slide, rocking or slide-rocking and overturning or falling of the body occur. Results are found for several values of parameters ε, T and λ.

5.3.1 Impulsive excitation

A horizontal impulsive ground excitation is considered individually in the following. Maps describing the criteria for the different phases of motion are obtained for base isolated non-symmetric rigid body subjects to a horizontal ground impulsive excitation and comparison between not isolated and isolated systems is carried out. These criteria maps are behaviour maps that divides the parameter plane ($I - \mu_s$) in different regions where the motion starts with a different phase of motion. Conditions where there is a rocking motion will be evaluated only referring to a rocking around corner 1 and $\varepsilon < 0$. This is possible since, as already pointed out, the system exhibits a symmetry in the rocking motion. Considering sliding condition given by Eq.(15) (with $\ddot{u}_g = \ddot{v}_g = 0$) and taking into account Eq.(35) and Eq.(37), it is possible to obtain the starting condition of the sliding motion:

$$C_S : |I| = \mu_s \frac{T g}{2\pi a(\xi)} \tag{38}$$

Starting rocking condition is still expressed by Eq.(37). By equating Eqs.(37, 38) it is possible to obtain the curve where, during rocking motion, the starting condition of sliding motion also becomes true:

$$C_{SR} : \mu_s = \frac{1}{\lambda}(1+\varepsilon) \tag{39}$$

When $\mu_s > (1+\varepsilon)/\lambda$ only the rocking motion is allowed (case considered in section 5.2). In order to find the condition at which a slide-rocking motion occurs starting from a pure rocking phase Eq.(18) must be taken into account. At the beginning of a rocking motion it can be considered that $\vartheta = \dot{\vartheta} = 0$ and, by referring to Fig.3(a), $b_1' = b_1$, $h_1' = h$. From Eq.(8_2) (with $\ddot{u}_g = \ddot{v}_g = 0$) it is possible to obtain the maximum angular acceleration $\ddot{\vartheta}_{\max}$:

$$\ddot{\vartheta}_{\max} = |I| \frac{2\pi m a(\xi) h}{T I_1} - \frac{m g b_1}{I_1} \tag{40}$$

where use of Eq.(35) is done. The curve along which a sliding motion occurs starting to a rocking phase can be obtained by Eq.(18), by taking into account Eq.(12), Eq.(19) and Eq.(40). It reads:

$$C_{RS} : \mu_s = \frac{|I|(3+6\varepsilon+3\varepsilon^2+\lambda^2)\omega a(\xi) + 3g(1+\varepsilon)\lambda}{\lambda[3|I|(1+\varepsilon)\omega a(\xi) + 4g\lambda]} \tag{41}$$

where use of Eq.(27) is done. Previous curves divide the parameter plane in several regions as shown in Fig.11(b)-(f). It is possible to observe that, when a base isolation is applied to the rigid body, a full-contact region appears.

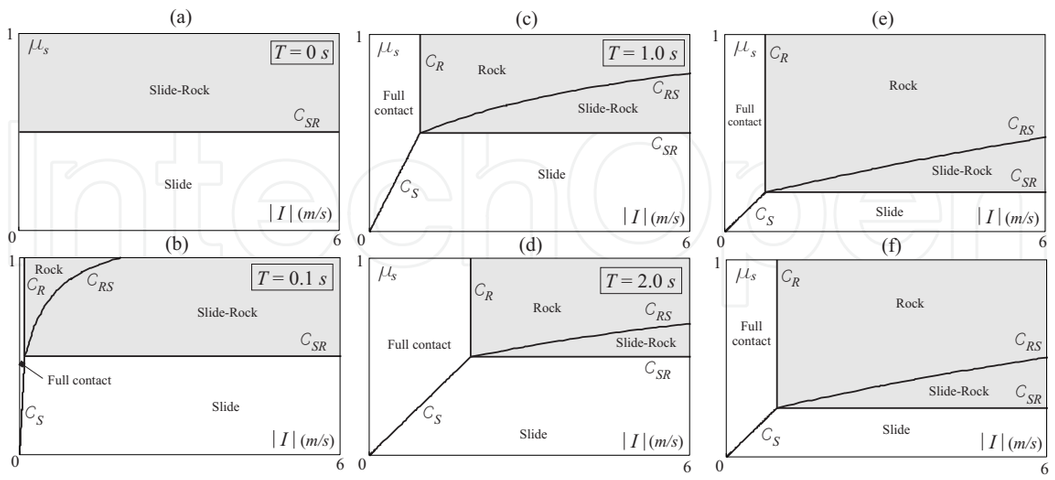

Fig. 11. Criteria maps: (a) not isolated system ($\lambda = 3,\ \varepsilon = 0,\ T = 2s$); (b) isolated system ($\lambda = 3,\ \varepsilon = 0,\ T = 0.1s$); (c) isolated system ($\lambda = 3,\ \varepsilon = 0,\ T = 1s$); (d) isolated system ($\lambda = 3,\ \varepsilon = 0,\ T = 2s$); (e) isolated system ($\lambda = 5,\ \varepsilon = 0,\ T = 2s$); (f) isolated system ($\lambda = 3,\ \varepsilon = -0.5,\ T = 2s$); ($\xi = 0.20$).

By considering the rocking motion particularly dangerous for the body, it is possible to observe that by increasing the period T of the oscillating base, the regions where there is rocking (grey regions) decrease (Fig.11(b)-(d)). By referring to the case where $T = 2s$ (Fig.11(d)), both an increase of the slenderness λ (Fig.11(e)) and of the eccentricity ε (Fig.11(f)) cause a deterioration in the performance to the system, since a reduction of the full-contact region and an increase of the rocking regions are observed.

5.3.2 Seismic excitation

In the numerical simulations performed here, $\mu_k = 0.8\,\mu_s$ is always used as in [Shenton & Jones, 1991]; according to results found in [Caliò & Marletta, 2003] and [Contento & Di Egidio, 2009], in this paper, it is always assumed $\xi = 0.2$. Where the security stop collision is concerned, $u_{\max} = 0.2m$, $\hat{x} = 0.1m$ and the restitution coefficients $\eta_{i,s} = 0.7$ are always chosen. In the following figures, these graphic conventions are always used: dashed curves are related to sliding motion and in particular heavy dashed curves are the curves at which a sliding motion begins, while thick dashed curves are the collapse curves due to the precipitation of the rigid block from the oscillating base; solid curves are related to rocking motion and in particular heavy solid curves are the curves at which rocking begins, while thick solid curves are the collapse curves due to overturning of the rigid body. Finally heavy dotted curves refer to the reaching of a slide $x = \hat{x}$ above which the body is partially out of the oscillating base, thick dotted curves refer to a collision with the slide security stops and thick dash-dot curves refer to a collision with the base isolation security stops when they are considered.

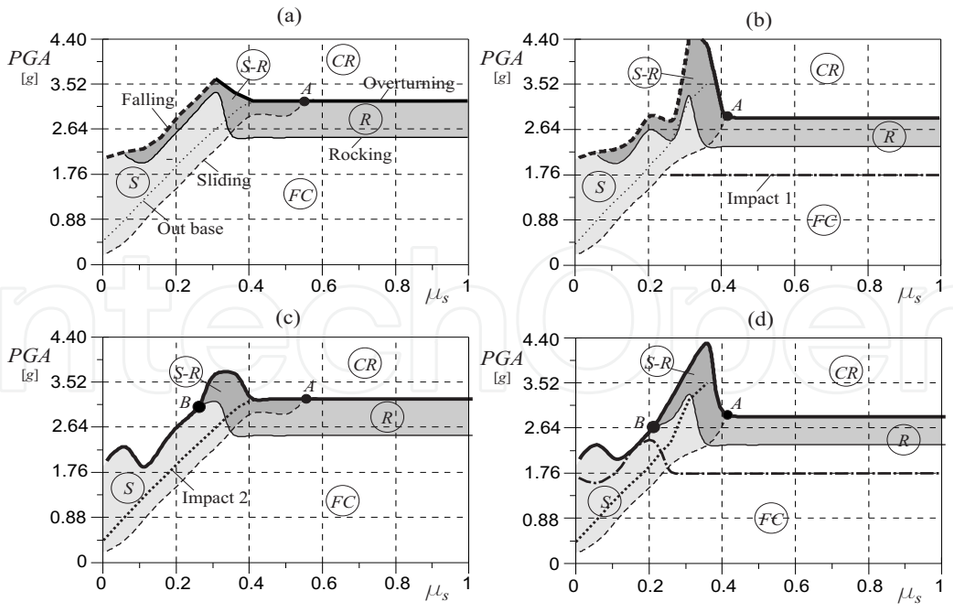

Fig. 12. Seismic analysis under Brienza earthquake: (a) *PGA* versus static friction coefficient μ_s - no security stops; (b) *PGA* versus static friction coefficient μ_s - only base stops; (c) *PGA* versus static friction coefficient μ_s - only sliding stops; (d) *PGA* versus static friction coefficient μ_s - both base and sliding stops; ($\lambda = 3$, $\varepsilon = 0$, $T = 2s$).

Results of the first analysis are shown in Fig.12 where the *PGA* associated with the first occurrence of sliding, rocking, falling or overturning is plotted versus the static friction coefficient μ_s, under Brienza earthquake for a body with slenderness $\lambda = 3$ and eccentricity $\varepsilon = 0$. In each graph of Fig.13 it is possible to observe the existence of five different regions: a region *S* where only sliding motion can occur, a region *S-R* where rocking or slide-rocking motion can occur, a region *R* of pure rocking motions, a region *FC* where during the motion the body and the base remain in full contact and a critical region *CR*. Here, as for the rocking case, the survival regions could exist. At the labelled point *A* a collision between the sliding curve and the overturning one manifests itself. While the sliding curve and the critical falling curve strongly depend on the friction coefficient μ_s, it is very interesting to note that the rocking and the overturning curve are practically independent from μ_s above the point *A*. As observed in [Di Egidio & Contento, 2009] in this region, where the behaviour of the system does not depend on the friction, only a pure rocking motion is possible. Differently from the results obtained in [Di Egidio & Contento, 2009] where the body could not exit from the oscillating base, here, also for small values of the static friction coefficient, a rocking motion manifests itself. This is possible since, when the body is out the base (this happens over the curve labelled Out base), it can rock easily because the resisting moment becomes smaller and smaller as the body comes out the base (see Figs. 12(a),(b)). The effects of the presence of the security stops on the behaviour of the system are very interesting. Figure 12(a) refers to the absence of these stops. When security stops on oscillating base are considered (Fig.12(b)) a worsening of the performance of the system in the *R* region can be observed, because rocking and overturning can occur for smaller values of the *PGA*. On the contrary, around the conjunction between the falling and the overturning curves it is possible to observe an improvement of the performance of the system. It is useful to note for next comments, that the impact on the security stops (above the curve labelled Impact 1) happens before a rocking motion manifests itself. The introduction of security stops on the sliding motion (Fig.12(c), curve labelled Impact 2) change the falling collapse events in overturning collapse events. Since below the point *B* rocking and overturing curves coincide, rocking and overturning events happen for the same *PGA* and no *S-R* region exists. However the presence of these kind of security stops, do not change significantly the values of *PGA* at which a collapse can occur. Finally in Fig.12(d) results obtained from the contemporary presence of the two kind of security stops are shown.

The effects of the eccentricity and specially of the slenderness on the performance of the system are shown in Fig.13. In Figs. 13(a)-(d) the results obtained for a body with slenderness $\lambda = 3$ and eccentricity $\varepsilon = 0.35$ are reported. First of all the worsening of the behaviour of the system due to an increasing of the eccentricity with respect to the results shown in Fig.12 must be observed, since smaller *PGA* are now able to cause falling and overturning collapse events. Another interesting aspect is related to the presence of security stops on the oscillating base (Fig.13(b)). Due to the increased eccentricity, the rocking starts before a collapse on security stops happens. This fact makes the system less sensitive to the presence of this kind of security stops compared to the case analyzed previously and shown in Fig.12. The presence of the security stops on the sliding motion (Fig.13(c)) or the contemporary presence of the two kind of security stops (Fig.13(d)) have, in this case, a

small impact on the performance of the system. On the contrary, in Figs. 13(e)-(h), results obtained for a lesser slenderness $\lambda = 2$ (and the same eccentricity $\varepsilon = 0.35$) are shown. First of all it must be observed that a decreasing of the slenderness causes a reduction of the region *R* where a pure rocking motion manifest itself, since the sliding motion becomes possible for higher values of the friction coefficient. By comparing results obtained without security stops (Fig.13(e)) and with only the security stops on the oscillating base (Fig.13(f)), it is possible to observe the great positive influence of this type of stops specially on the overturning collapse condition. The great sensitivity to the presence of these security stops is related to the fact that the impact on them happens before the rocking motion starts as observed also in the previous case.

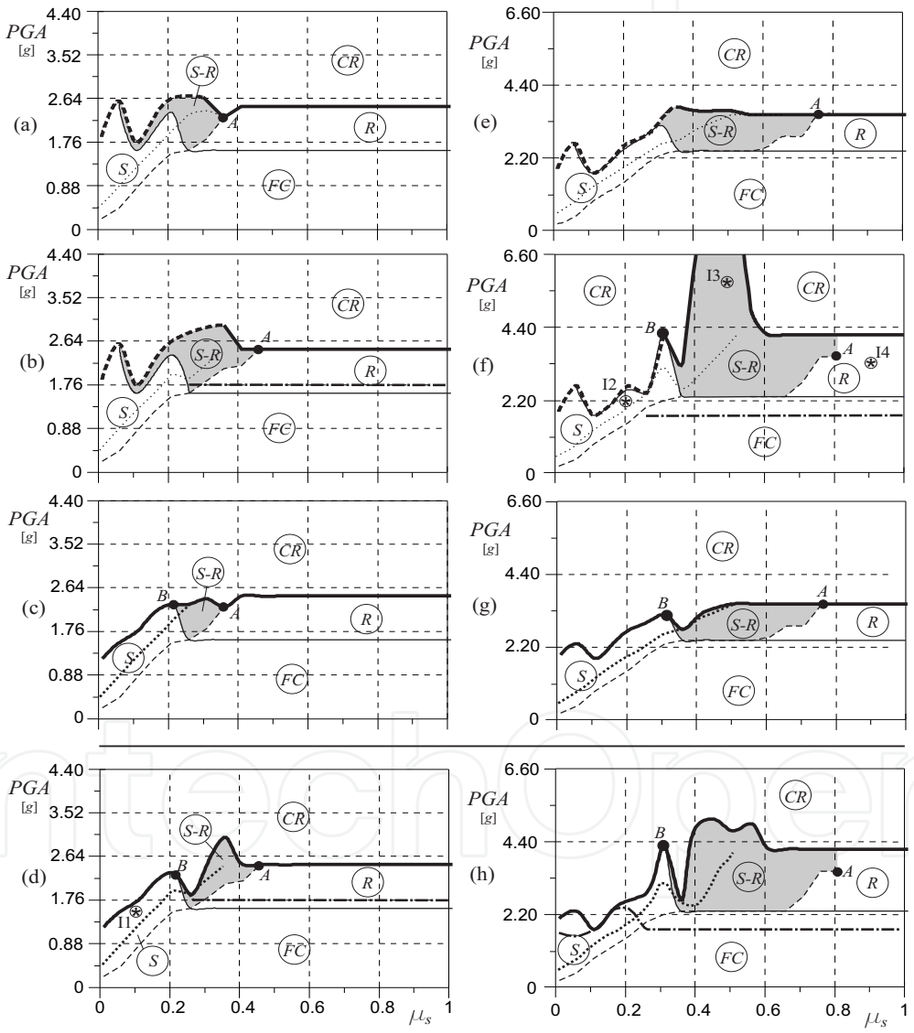

Fig. 13. Seismic analysis under Brienza earthquake: (a)-(d) *PGA* versus static friction coefficient μ_s ($\lambda = 3$); (a) no security stops; (b) only base stops; (c) only sliding stops; (d) both base and sliding stops. (e)-(h) *PGA* versus static friction coefficient μ_s ($\lambda = 2$); (e) no security stops; (f) only base stops; (g) only sliding stops; (h) both base and sliding stops; ($\varepsilon = 0.35$, $T = 2s$).

Unlike the case with $\lambda = 3$ (shown in Fig.12(b)), where security stops on an oscillating base cause a worsening of the performance of the system, for smaller slenderness they improve the behaviour of the system. The presence of security stops on sliding motion have a small impact on the behaviour of the system as shown in Fig.13(g). Finally the contemporary presence of the two types of security stops causes a general improvement of the performance of the system compared to their total absence. To conclude, the comparison between the case with $\lambda = 3$ (Figs. 13(a)-(d)) and $\lambda = 2$ (Figs. 13(e)-(h)) shows that the performances of the two system are similar as to the falling collapse conditions (when no security stops on sliding are considered), while in the overturning conditions the behaviour of the system with lesser slenderness is much better than the other one.

In Fig.14 some time-histories of different cases contained in different regions are shown. A case of pure slide motion in the presence of security stops is shown in Fig.14(a) for a point labelled with I1 in Fig.13(d). It is possible to observe the impossibility of the system to overcome the threshold value $|\hat{x}|$. When no sliding security stops are considered, the body can exit from the base as shown in Fig.14(b) for a point labelled I2 in Fig.13(f). In Fig.14(c) a case contained in the *S-R* region in presence of only security stops on the oscillation base is shown (point labelled I3 in Fig.13(f)). It is possible to observe the impacts of the oscillating base on the stops from the time-history of the displacement u that never exceed the threshold value $|u_{\max}|$. From the time-histories of x and ϑ two different slide-rocking motions can be observed. Below the time t_{SR}, as the body is inside the support, rocking or slide-rocking motion around the corners of the of the body manifest themselves; above the time t_{SR}, as the body is outside the support, rocking and slide-rocking motion happen around the corners of the support. In particular, in this last case the rocking motion happens around the left corner of the support since $-\hat{x} > x$ and the right corner of the body. In Fig.14(d) the time-histories of a pure rocking motion are finally shown (point labelled I4 in Fig.13(f)).

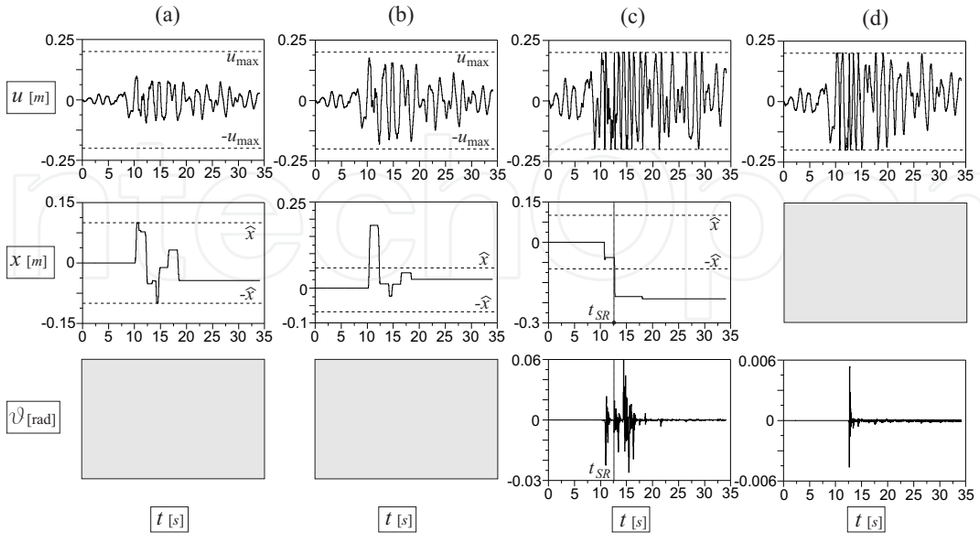

Fig. 14. Time-histories under Brienza earthquake: (a) system marked with I1 in Fig.13(d); (b) system marked with I2 in Fig.13(f); (c) system marked with I3 in Fig.13(f); (d) system marked with I4 in Fig.13(f).

In Figs. 15 results obtained for a body with slenderness $\lambda = 1$ and eccentricity $\varepsilon = 0.35$ are shown. It is very interesting to observe that in this case, the collapse of the system, also when no security stops are considered (Fig.15(a)), is related only to the overturning of the body. This fact can be explained by observing the great attitude of a body with less slenderness to slide instead of rocking. Since these kinds of bodies easily exit from the limits of the support by sliding and can easily reach large sliding displacement *x*, when a rocking motion starts, a overturning condition follows due to the small value of the resisting moment. When the two different security stops are considered a great improvement of the performance of the system is observed. This fact confirms the positive effects of the stops to system with a smaller slenderness. Above the points labelled with *C* rocking and sliding curves coincide. Finally it can be noted that no pure rocking region exists.

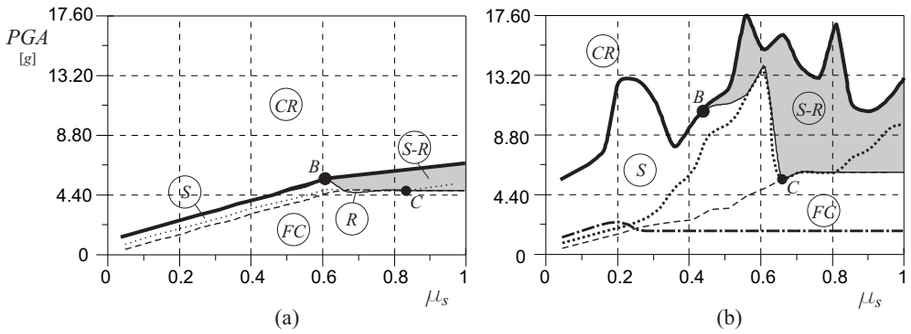

Fig. 15. Seismic analysis under Brienza earthquake, PGA vs static friction coefficient μ_s :(a) no security stops; (b) base and sliding stops; ($\lambda = 1,\ \varepsilon = 0.35,\ T = 2s$).

6. Conclusion

A model of a non-symmetric rigid body, where the centre of gravity is not equally distant from the two base corners can be used to investigate the behaviour of a real base isolated art object. The base under the rigid body is connected to the ground by a linear visco-elastic device representing the passive control system. Exact nonlinear equations of motion have been written by using a Lagrangian approach and transition conditions have also been derived. In the case in which no sliding security stops are considered original equations of motion describing the slide-rocking motion of the rigid block when it is partially outside the support have been obtained. For the impulsive excitation exact and approximated (for damped systems) results have been obtained in closed form while seismic excitation has been considered by using two Italian registered earthquakes. Two different kinds of collapse condition have been considered: the fall from the oscillating base of the rigid block and the overturning of the body. The analysis has been conducted with the aim of pointing out the effects of the friction coefficient, the influence of the slenderness and of the eccentricity of the body and the analysis confirms that base isolation can be more effective for rigid bodies with geometrical parameters similar to those of real works of art. Security stops have been considered one kind able to prevent isolation device breakage by limiting the displacement of the oscillating base to a maximum safety value, another introduced to prevent the rigid body from falling off the base. For wider bodies security stops turn out to have a positive influence on the performance of the system while above a certain value of slenderness they can worsen the behaviour of the system.

7. References

Agbabian M.S., Masri F.S., Nigbor R.L. & Ginel W.S. (1988). Seismic damage mitigation concepts for art objects in museum, *Proceeding of the 9th World Conference on Earthquake Engineering*, No.7, pp. 235-240, Tokyo-Kyoto, Japan, 1988

Batista M. (2006). Steady motion of a rigid disc of finite thickness on a horizontal plane. Journal of Nonlinear Mechanics, Vol.41, pp.850 – 859

Boroscheck R.L. & Romo D. (2004). Overturning criteria for non-anchored non-symmetric rigid bodies, *Proceeding of the 13th World Conference on Earthquake Engineering*, Vancouver, B.C., Canada, August 1-6, 2004

Caliò I. & Marletta M. Passive control of the seismic response of art objects. *Engineering Structures*, Vol.25, pp. 1009-1018

Contento A. & Di Egidio A. (2009). Investigations into Benefits of Base Isolation for Non-Symmetric Rigid Blocks. *Earthquake Engineering and Structural Dynamics*, Vol.38, pp. 849-866

Di Egidio A. & Contento A. (2009). Base Isolation of Sliding-Rocking Non-Symmetyric Rigid Blocks Subjected to Impulsive and Seismic Excitations. *Engineering Structures*, Vol.31, pp. 2723-2734

Di Egidio A. & Contento A. (2010). Seismic response of a non-symmetric rigid block on a constrained oscillating base. *Engineering Structures*, Vol.32, pp. 3028-3039

Fujita K., Yoshitomi S., Tsuji M. & Takewaki I. (2008). Critical cross-correlation function of horizontal and vertical ground motions for uplift of rigid block. *Engineering Structures*, Vol.30, No.5, pp.1199-1213

Koh A.S. & Mustafa G. (1990). Free rocking of cylindrical structures. *Journal of Engineering Mechanics*, Vol.116, pp.34 – 54

Kounadis A.N. (2010). On the overturning instability of a rectangular rigid block under ground excitation. *The Open Mechanics Journal*, Vol.4, pp. 43 – 57

Makris N. & Black C.J. (2004). Dimensional analysis of bilinear oscillators under pulse-type Excitations. *Journal of Engineering Mechanics* (ASCE), Vol.130, No.9, pp. 1019-1031

Pompei A., Scalia A. & Sumbatyan M. (1998). Dynamics of rigid block due to horizontal ground motion. *Journal of Engineering Mechanics*, Vol.124, No.7, pp. 713-717

Purvance M.D. (2005). Overturning of slender blocks: numerical investigation and application to precariously balanced rocks in southern California. Ph.D. Dissertation, University of Nevada, Reno, Available from http://www.seismo.unr.edu/PrecRock/gradresearch.html

Purvance M.D., Anooshehpoor A. & Brune J.N. (2008). Freestanding block overturning fragilities: Numerical simulation and experimental validation. *Earthquake Engineering and Structural Dynamics*, Vol.37, No.5, pp. 791-808

Shenton H.W. III. (1996). Criteria for initiation of slide, rock, and slide-rock rigid-body modes. *Journal of Engineering Mechanics* ASCE, Vol.122, No.7, pp. 690-693

Shenton H.W. & Jones N.P. (1991). Base excitation of rigid bodies. I: Formulation. *Journal of Engineering Mechanics*, Vol.117, No.10, pp. 2286-306

Stefanou I., Vardoulakis I. & Mavraganis A. (2011). Dynamic motion of a conical frustum over a rough horizontal plane. *International Journal of Non Linear Mechanics*, Vol.46, pp.114 – 124

Taniguchi T. (2002). Non-linear response analyses of rectangular rigid bodies subjected to horizontal and vertical ground motion. *Earthquake Engineering and Structural Dynamics*, Vol.31, pp. 1481-1500

Taniguchi T. (2004). Rocking behavior of unanchored flat-bottom cylindrical shell tanks under action of horizontal base excitation. *Engineering Structures*, Vol.26, pp.415 – 426

Tung CC. (2007). Initiation of motion of a free-standing body to base excitation. *Earthquake Engineering and Structural Dynamics*, Vol.36, pp. 1431-1439

Vassiliou M.F. & Makris N. (2011). Analysis of the rocking response of rigid blocks standing free on a seismically isolated base. *Earthquake Engineering and Structural Dynamics,* DOI: 10.1002/eqe.1124

Vestroni F. & Di Cinto S. (2000). Base isolation for seismic protection of statues, *Proceeding of the 12th World Conference on Earthquake Engineering*, New Zeland, 2000.

Zhang J. & Makris N. (2001). Rocking Response of Free-Standing Blocks Under Cycloidal Pulses. *Journal of Engineering Mechanics,* Vol.127, No.5, pp. 473-483

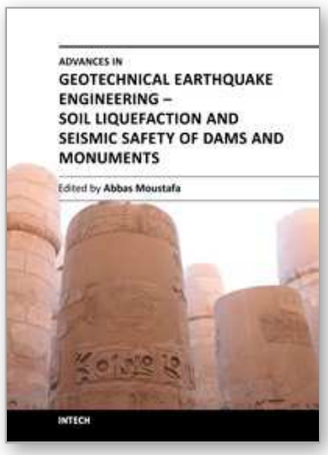

Advances in Geotechnical Earthquake Engineering - Soil Liquefaction and Seismic Safety of Dams and Monuments

Edited by Prof. Abbas Moustafa

ISBN 978-953-51-0025-6
Hard cover, 424 pages
Publisher InTech
Published online 10, February, 2012
Published in print edition February, 2012

This book sheds lights on recent advances in Geotechnical Earthquake Engineering with special emphasis on soil liquefaction, soil-structure interaction, seismic safety of dams and underground monuments, mitigation strategies against landslide and fire whirlwind resulting from earthquakes and vibration of a layered rotating plant and Bryan's effect. The book contains sixteen chapters covering several interesting research topics written by researchers and experts from several countries. The research reported in this book is useful to graduate students and researchers working in the fields of structural and earthquake engineering. The book will also be of considerable help to civil engineers working on construction and repair of engineering structures, such as buildings, roads, dams and monuments.

InTech Europe
University Campus STeP Ri
Slavka Krautzeka 83/A
51000 Rijeka, Croatia
Phone: +385 (51) 770 447
Fax: +385 (51) 686 166
www.intechopen.com

InTech China
Unit 405, Office Block, Hotel Equatorial Shanghai
No.65, Yan An Road (West), Shanghai, 200040, China
中国上海市延安西路65号上海国际贵都大饭店办公楼405单元
Phone: +86-21-62489820
Fax: +86-21-62489821

IntechOpen